Spin-to-charge conversion and interface-induced spin Hall magnetoresistance in yttrium iron garnet/metallic bilayers

Holanda, J.; Santos, O. Alves; Mendes, J. B.S.; Rezende, S. M.

Published in:
Journal of Physics Condensed Matter

DOI:
10.1088/1361-648X/ac16f7

Publication date:
2021

PAPER

Spin-to-charge conversion and interface-induced spin Hall magnetoresistance in yttrium iron garnet/metallic bilayers

IOP Publishing Journal of Physics: Condensed Matter
J. Phys.: Condens. Matter **33** (2021) 435803 (7pp) https://doi.org/10.1088/1361-648X/ac16f7

Spin-to-charge conversion and interface-induced spin Hall magnetoresistance in yttrium iron garnet/metallic bilayers

J Holanda[1,*], O Alves Santos[2], J B S Mendes[3] and S M Rezende[4]

[1] Departamento de Física, Universidade Federal do Espírito Santo, 29075-910, Vitória, ES, Brazil
[2] Physics of Nanodevices, Zernike Institute for Advanced Materials, University of Groningen, Nijenborgh 4, Groningen, AG 9747, The Netherlands
[3] Departamento de Física, Universidade Federal de Viçosa, 36570-900 Viçosa, MG, Brazil
[4] Departamento de Física, Universidade Federal de Pernambuco, 50670-901, Recife, PE, Brazil

E-mail: joseholanda.papers@gmail.com and jose.silva.04@ufes.br

Received 27 May 2021, revised 13 July 2021
Accepted for publication 22 July 2021
Published 13 August 2021

Abstract

We report the investigation of spin-to-charge current interconversion process in hybrid structures of yttrium iron garnet (YIG)/metallic bilayers by means of two different experimental techniques: spin pumping effect (SPE) and spin Hall magnetoresistance (SMR). We demonstrate the evidence of a correlation between spin-to-charge conversion and SMR in bilayers of YIG/Pd, YIG/Pt, and YIG/IrMn. The correlation was verified directly in the spin Hall angles and the amplitudes of the voltage signals measured by the SPE and SMR techniques. The detection of SMR was carried out using the modulated magnetoresistance technique and lock-in amplifier detection. For these measurements, we present a simple model for the interpretation of the results. The results allow us to conclude that indeed the interface in the YIG/metallic bilayers has a dominant role in the spin-to-charge current conversion and SMR.

Keywords: spin, charge, conversions, interface-induced, Hall

(Some figures may appear in colour only in the online journal)

1. Introduction

The conversion of signals carried by spin excitations in ferromagnets (FMs) is a key phenomenon for the feasibility of spintronics-based devices for new information-age technologies [1–5]. In bilayers of FMs with metallic layers (MLs), the spin excitations can create a pure spin current on the MLs by means of different methods, such as the spin pumping effect (SPE), which injects a spin current by the precession of spins in the FM layer at the ferromagnetic resonance (FMR) condition [1–17]. Once the spin current enters into the MLs, the spin-to-charge conversion can occur by means of the inverse spin Hall effect (ISHE), generating a voltage at the edges of the MLs. This phenomenon was first investigated using permalloy as FM layer and MLs of materials with high spin–orbit coupling, such as platinum (Pt) and tantalum (Ta) [7, 8]. Recently it has been shown how the FMR of permalloy is modulated by spin Hall effects in adjacent epitaxial $IrMn_3$ films. The authors observed a large DC modulation of the FMR linewidth for currents applied along the [001] $IrMn_3$ direction. This very strong angular dependence of spin–orbit torques from DC currents through the bilayers was explained by the magnetic spin Hall effect where $IrMn_3$ provides novel pathways for modulating the magnetization dynamics electrically [18]. The studies about SPE-ISHE were boosted by the observation of the SPE in the ferrimagnetic insulator yttrium iron garnet (YIG) [19].

* Author to whom any correspondence should be addressed.

Nowadays, most experiments are carried out with YIG films as the FM layer, mainly because of its very low magnetic damping, large magnon propagation length, and the fact that YIG has an electronic energy gap of approximately 3 eV, which also opens opportunities for opto-spintronics [20, 21].

The ML has a key role in several spintronic phenomena, thus it is important to study the characteristics of interfaces of ML in contact with FM materials. It is well known that the conducting and magnetic properties of MLs are overwhelmed by the FM properties close to the FM/ML interface, such as the proximity effect [22–25]. The conducting and magnetic properties of the ML deposited on an insulator can be determined readily through transport measurements. One of the ways to access these properties in an ML in contact with an FM insulator is through its spin Hall magnetoresistance (SMR) [16, 22]. Another independent technique to probe the properties of the ML and the interface is the microwave driven spin-pumping SPE-ISHE. This paper reports a comparative study of the spin-to-charge current conversion in three different metals, Pd, Pt, and IrMn, carried out with two independent techniques, microwave spin pumping and SMR. The measurements were made at room temperature in bilayers of YIG/Pd, YIG/Pt, and YIG/IrMn. The values of the spin Hall angle obtained with the two techniques, SPE-ISHE and SMR, are in good agreement for Pt, but not for Pd and IrMn. Possible reasons for the discrepancies in Pd and IrMn are discussed.

2. Experiments

The FM samples were obtained from a single-crystal YIG film with a thickness of 7.0 μm grown by liquid-phase epitaxy onto a 0.5 mm thick substrate of (111) gallium gadolinium garnet (GGG). All samples were cut from the same GGG/YIG wafer in rectangular shape 1.4 $\times$ 3.2 mm^2, with the long dimension in a $\langle 111 \rangle$ axis. The good quality of the YIG films is demonstrated by the very small FMR linewidth of the bare YIG films, about 0.5 Oe. Any chemical composition different from $Y_3Fe_5O_{12}$, or crystal phase different from the garnet phase, results in larger linewidths. The surfaces of the YIG films were cleaned in ultrasound baths of acetone and isopropanol for 30 min and dried in nitrogen gas jet. Here we did not use any treatment to modify the YIG single crystal surface, as was done in the references [26–28]. Nominally 4 nm thick layers of Pd, Pt, and IrMn were deposited on the YIG film using a DC sputtering technique, followed by wire bonding of two contacts, as illustrated in figure 1. The deposition and characterization process of the IrMn films are described in reference [29]. Figure 1(a) illustrates the spin-to-charge conversion in the SPE-ISHE experiments, and figure 1(b) illustrates the mechanism of the SMR. The crystallographic structure of the YIG was assessed by x-ray diffraction (XRD) measurements. The XRD patterns were recorded using the Bruker D8 Discover diffractometer equipped with Cu $K\alpha$ radiation ($\lambda = 1.5418$ Å). The XRD scan pattern (θ–2θ) is shown in figure 1(c). The diffraction patterns were obtained at angles between 10° and 90° (2θ). Only the characteristic peak at $2\theta \approx 51.2^{\circ}$ associated with the (444) crystal plane of YIG appears in the out-of-plane XRD pattern, indicating that no impurity phases precipitated. The XRD spectrum at high resolution detailing the position of the peaks of the YIG film and the GGG substrate is shown in the insert. The results of XRD measurements indicate that the present YIG film is epitaxially grown on the GGG substrate.

All measurements reported here were carried out at room temperature. In the SPE-ISHE experiments a microwave magnetic field drives the FMR in the FM insulator and the magnetization precession produces a spin current across the FM/ML interface by the spin pumping process. On the other hand, in the SMR, a DC electric current I_{DC} applied between the two electrodes creates a spin current by the spin Hall effect, that flows into the FM, inducing a spin pumping back into the ML, that produces a change in its resistance ΔR that varies with the applied magnetic field. Here we have used an AC modulation field super imposed to the static field, both perpendicular to the sample-long dimension, so that the change in resistance generates an AC voltage that is measured with a lock-in amplifier. This modulation technique allows the investigation of very weak magnetoresistances (MRs) [16].

In the SPE-ISHE experiments, the YIG/MLs samples are submitted to a microwave magnetic field perpendicular to the static field at the FMR condition. The YIG/ML bilayer sample with the two electrodes is mounted on top of a PVC rod with a protractor in the base. The rod with the sample is inserted into a small hole in the back wall of a shorted X-band microwave waveguide, at a point of maximum microwave magnetic field and zero electric field. The waveguide is inserted between the poles of an electromagnet so that sample can be rotated with the protractor while maintaining the applied static field and rf magnetic field in the film plane and perpendicular to each other. The ISHE voltage resulting from the spin-to-charge conversion is detected by the electrodes as sketched in figure 1(a), connected directly to a nanovoltmeter. The V_{ISHE} spectrum is obtained by sweeping applied magnetic field H sweep and using no AC modulation field. The protractor with the sample is rotated to measure the voltage dependence on the angle ϕ, shown in figure 1(a). The measurements were carried out at a fixed microwave frequency of 9.4 GHz and incident power of 78 mW.

In the SMR experiments, an important aspect is the resistance change as a function of the applied magnetic field H. It is well known that the SMR results from a small change in resistance, so the modulated resistance technique (MRT) is an ideal technique to observe this effect because it detects signals with small amplitudes and averts the small external magnetic perturbations [16]. Detection of the signal generated by MRT is made using a lock-in amplifier. A constant DC electric current of 60 μA is injected into the YIG/ML bilayer while under an AC modulation magnetic field with amplitude $H_{Mod} = 0.3$ Oe and frequency 4.4 kHz. The change in resistance $\Delta R = \Delta V/I$ as a function of the applied magnetic field H is obtained from the voltage ΔV measured in the lock-in amplifier.

3. Models

Spin pumping-ISHE: in a microwave spin pumping process, the spin current produced by the precessing spins produces two effects: (1) Increased damping relative to the single FM

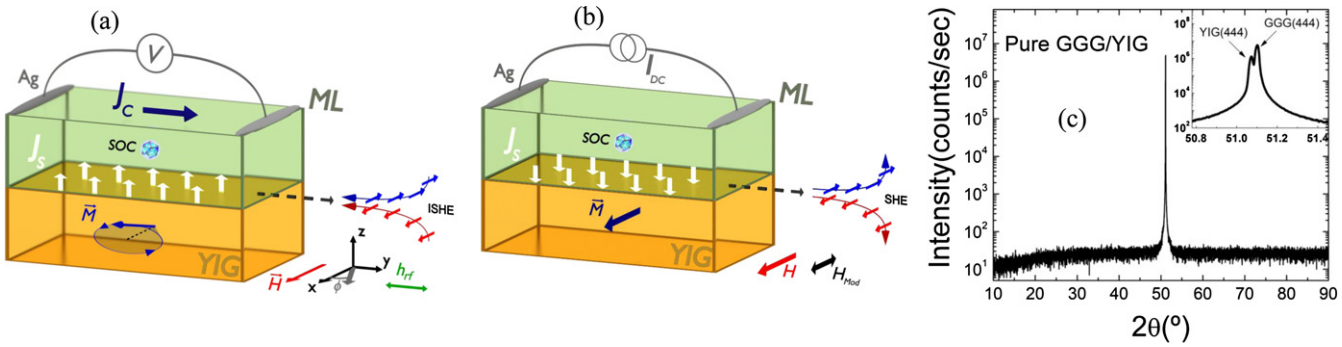

Figure 1. Experimental setup for SPE-ISHE and SMR measurements in YIG/ML bilayers with Pd, Pt, and IrMn, showing the electrodes used in each case and total magnetic field $H_T = H + H_{Mod}$, where H is the applied magnetic field and H_{Mod} is the AC modulation field. (a) Schematic sketch of the arrangement used for measuring the ISHE voltage produced by the microwave driven spin pumping process. (b) Schematic sketch of the arrangement used to apply the DC electric current I_{DC} to measure the MR ΔR. (c) XRD patterns (θ–2θ scans) of YIG film grown on GGG substrate. The XRD spectrum at high resolution detailing the positions of the peaks of the YIG film and the GGG substrate is shown in the inset.

due to the out flow of angular momentum; (2) spin-to-charge conversion by the ISHE in the ML creating a voltage between the two electrodes [1–6]. One can write the spin current density at the YIG/ML interface produced by the precession of the magnetization M of the YIG as [1]

$$\vec{J}_S = \left[\frac{2hg_r^{\uparrow\downarrow}}{(4\pi M)^2}\right]\left(\vec{M}\times\frac{\partial\vec{M}}{\partial t}\right), \tag{1}$$

where h is Planck's constant and $g_r^{\uparrow\downarrow}$ is the real part of the interface spin-mixing conductance, including the back-flow effect. The spin-pumped spin current density at the YIG/ML interface produced by the YIG magnetization precession is

$$J_S = \frac{hfpg_{eff}^{\uparrow\downarrow}}{4\pi}\left(\frac{h_{mw}}{\Delta H_{YIG/ML}}\right)^2 L(H-H_R), \tag{2}$$

where f and h_{mw} are the frequency and amplitude of the driving microwave magnetic field, respectively, $\Delta H_{YIG/ML}$ is the half-width at half-maximum (HWHM) of the YIG/ML bilayer, L(H – H_R) denotes a Lorentzian function, H_R is the field for resonance, p is the precession ellipticity factor given by $p = 4\left(f/\gamma\right)\left(H_R + 4\pi M_{eff}\right)/\left(2H_R + 4\pi M_{eff}\right)^2$ and $g_{eff}^{\uparrow\downarrow}$ is the real part of the effective spin mixing conductance. This quantity can be determined with from measurements of the FMR linewidths using the expression $g_{eff}^{\uparrow\downarrow} = \left(4\pi M_{eff} t_{coh}/hf\right)\left(\Delta H_{YIG/ML} - \Delta H_{YIG}\right)$, where $4\pi M_{eff} = \left[\left(f/\gamma H_R\right)^2 - 1\right] H_R$ is the effective magnetization that is obtained from FMR condition ($H = H_R$), t_{coh} is the coherence length representing an effective thickness of the YIG film [16], $\gamma = 2.8$ GHz kOe^{-1} is the gyromagnetic ratio for YIG, and ΔH_{YIG} is the HWHM of the bare YIG film. Note that equation (2) gives J_S in units of angular momentum/time area [1–6, 16]. In the ML, the ISHE mechanism converts the spin current into charge current given by $\vec{J}_C = \theta_{SH}\left(4\pi e/h\right)\vec{J}_S \times \hat{\sigma}$, where θ_{SH} is the spin Hall angle, e is the electron charge, and $\hat{\sigma}$ is the spin polarization determined by the direction of the applied field. Integration of $\vec{J}_C$ gives for the ISHE voltage

$$V_{ISHE} = R_{ML} w \lambda_{ML} \frac{4\pi e}{h}\theta_{SH}\tanh\left(\frac{t_{ML}}{2\lambda_{ML}}\right)(\cos\phi) J_S, \tag{3}$$

where R_{ML}, t_{ML}, w, and λ_{ML} are the resistance, thickness, width, and spin diffusion length of the ML, respectively, and J_S is the spin current density given by equation (2) at the interface. By using equations (2) and (3), at the FMR condition one can calculate the spin Hall angle with

$$\theta_{SH} = \frac{4hV_{ISHE}^{Peak}}{4\pi M_{eff} t_{YIG} w N R_{ML} e p_{y,z} h_{mw}^2 (\cos\phi)} \times \left[\frac{\left(\Delta H_{YIG/ML}\right)^2}{\Delta H_{YIG/ML} - \Delta H_{YIG}}\right], \tag{4}$$

where, $N = \lambda_{ML}\tanh\left(t_{ML}/2\lambda_{ML}\right)$, $p_{y,z}$ is a factor that represents the characteristic of ellipticity and the spatial condition of the FMR mode and microwave magnetic field is $h_{mw} = 2P^{1/2}/(f\mu_0\lambda_g ab)^{1/2}$, where P is the microwave power, λ_g, and a and b are the guide wavelength and the two inner waveguide dimensions, and μ_0 represent the vacuum permeability.

Spin Hall magnetoresistance: the magnetic field and temperature dependences of the MR in many magnetic metals can be analyzed in terms of Kohler's rule [30, 31]

$$MR = \frac{R(H,T) - R(0,T)}{R(0,T)} = F\left(\frac{H,M}{R(0,T)}\right), \tag{5}$$

where M is the magnetization of the FM material, while $R(H, T)$, and $R(0, T)$ are the resistances with and without applied magnetic field, respectively. For the modulated SMR F can be written as

$$F\left(\frac{H,M}{R(0,T)}\right) = \left(\frac{H_{Mod}}{R(0,T)}\right)\left(\frac{dR(H,T)}{dH}\right). \tag{6}$$

On other hand, by the theory of the SMR in FM/ML bilayers, the transverse component of the maximum change of SMR

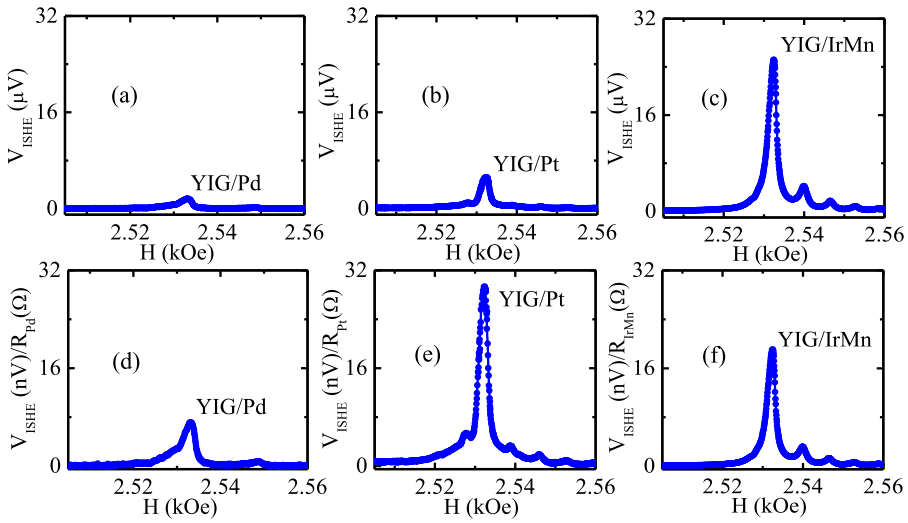

Figure 2. Field scan spectra of the SPE-ISHE DC voltage measured with a microwave frequency $f = 9.4$ GHz and input power 78 mW in YIG/ML bilayers. (a) YIG/Pd, (b) YIG/Pt, and (c) YIG/IrMn. The charge current field scan spectra for the three bilayers: (d) YIG/Pd, (e) YIG/Pt, and (f) YIG/IrMn.

is given by [32, 33]

$$\frac{R(H,T) - R(0,T)}{R(0,T)} = \theta_{SH}^2 \left[\left(\frac{\lambda_{ML}}{t_{ML}} \right) \tanh \times \left(\frac{t_{ML}}{\lambda_{ML}} \right) \tan h^2 \left(\frac{t_{ML}}{2\lambda_{ML}} \right) \right]. \quad (7)$$

From equations (5)–(7), we obtain an expression to calculate the spin Hall angle from the MR measured using the modulated MR technique

$$\theta_{SH} = \left\{ \left[\left(\frac{H_{Mod}}{R_{ML}} \right) \left(\frac{dR(H,T)}{dH} \right) \right] \left[\left(\frac{t_{ML}}{\lambda_{ML}} \right) \coth \times \left(\frac{t_{ML}}{\lambda_{ML}} \right) \cot h^2 \left(\frac{t_{ML}}{2\lambda_{ML}} \right) \right] \right\}^{1/2}, \quad (8)$$

where R_{ML} is the resistance at room temperature.

4. Results and discussions

The YIG/Pd and YIG/IrMn measurements are systematically compared to the data in YIG/Pt since this bilayer is one of the standard systems due to its high efficiency for spin-to-charge interconversion [2]. As discussed above and illustrated in figure 1, the SPE and SMR experiments can be readily used to investigate the spin-to-charge conversion by means of two independent processes. Here, the two phenomena suit to analyze mainly the correlation between them. Figure 2 presents the spectra of V_{ISHE} obtained with a microwave frequency of $f = 9.4$ GHz and an incident power of 78 mW, for a field applied in the direction $\phi = 0°$. The spectra exhibit large peaks under FMR conditions, and other small peaks due to volume and surface spin-wave modes [9, 10, 33]. The ISHE voltage peaks in the three samples differ in amplitude mainly due to the difference in the resistivity of the MLs. Division of the voltages by the resistances shows that all ISHE currents have roughly the same order of magnitude, as shown in figures 2(d)–(f).

The FMR HWHM for the bare YIG films used here was $\Delta H_{YIG} = 0.5$ Oe, measured at a frequency $f = 9.4$ GHz and input microwave power 38 mW using a shorted waveguide setup. The FMR linewidths measured after deposition of the ML, shown in table 1, were used to calculate the effective spin-mixing conductance for each bilayer. The linewidth from SPE-ISHE DC voltage represents the average of the linewidths of all magnetostatic modes in addition to the uniform mode. The values of the spin Hall angles θ_{SH} were determined with equation (4) for the three YIG/ML bilayer samples using the following parameter values: $p_{1,1} = 0.31$ for the uniform mode (1, 1); $4\pi M_S \approx 4\pi M_{eff} = 1.76$ kG; $t_{coh} \approx 100$ nm [16]; ML width $w = 1.4$ mm; thickness $t_{ML} = 4$ nm. Also, using the electromagnetic field in the TE_{10} mode for rectangular X-band waveguide, it is possible to calculate the microwave magnetic field $h_{mw} \approx 4 \times 10^{-2}$ Oe for a microwave power of 78 mW. With these parameters we obtain the spin Hall angle θ_{SH} for each of the three bilayer samples using equation (4) with $\phi = 0°$, shown in table 1. Comparison between the values of the measured voltage peaks in figure 2 gives $V^{Peak}_{YIG/Pt} \approx 3.25\ V^{Peak}_{YIG/Pd} \approx 0.2\ V^{Peak}_{YIG/IrMn}$. On the other hand, from the values of the calculated spin Hall angles, it is possible to write the following relation $\theta_{SH\text{-}Pt} \approx 3.92\ \theta_{SH\text{-}Pd} \approx 1.24\ \theta_{SH\text{-}IrMn}$. The results obtained for the voltage peaks and the spin Hall angle are in agreement with values reported in the literature [1–7, 18] and confirm the good quality of the interfaces of the YIG/ML bilayer samples used here.

In order to interpret the SMR data we have measured the magnetization versus field curve of the YIG/ML samples using a magneto-optical Kerr effect (MOKE) magnetometer. Figure 3(a) shows the data for YIG/Pt, that is essentially indistinguishable from the other samples. As is well known, YIG has a very small hysteresis, consequently, the reversal of the magnetic field produces an almost identical curve. Figure 3(b) shows the modulus of $M(dM/dH)$, calculated from the $M(H)$ data points from figure 1(b). This quantity expresses

Table 1. Parameters for the YIG/ML bilayers. The values of the spin Hall angle θ_{SH} were calculated with equation (4) from the SPE-ISHE measurements, and with equation (8) from the SMR measurements.

	YIG/Pd	YIG/Pt	YIG/IrMn
R_{ML}(Ohm)	230	178	1320
λ_{ML} (nm)	3.00	10.0	5.00
$\Delta H_{YIG/ML}$ (Oe)	1.20 ± 0.04	1.10 ± 0.03	0.85 ± 0.02
$V^{Peak}{}_{ISHE}$ (μV)	1.60 ± 0.03	5.20 ± 0.03	25.7 ± 0.02
SMR_{Peak}	$(2.00 \pm 0.003) \times 10^{-4}$	$(0.62 \pm 0.002) \times 10^{-4}$	$(0.12 \pm 0.003) \times 10^{-4}$
ISHE-θ_{SH} (%)	1.30 ± 0.05	5.10 ± 0.04	4.10 ± 0.03
SMR-θ_{SH} (%)	3.10 ± 0.03	4.10 ± 0.03	1.10 ± 0.02

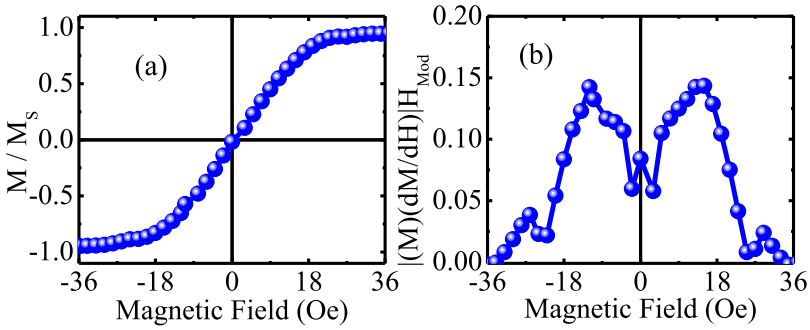

Figure 3. (a) Magnetization curve of YIG/Pt sample measured with scanning magnetic field applied in the film plane measured by the MOKE technique. (b) Plot of $|(M)\left(\mathrm{d}M/\mathrm{d}H\right)|H_{\mathrm{Mod}}$ versus magnetic field H calculated from the M versus H data in (a).

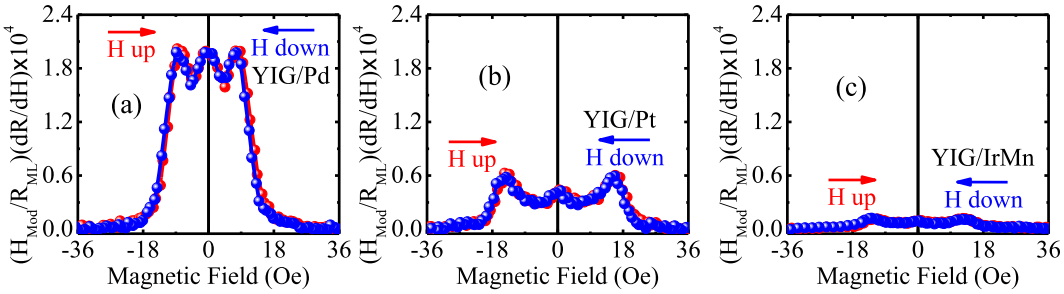

Figure 4. Field derivative of the resistance of the YIG/ML bilayers measured with scanning magnetic field H, using AC magnetic field modulation with $H_{\mathrm{Mod}} = 0.3$ Oe at a frequency of 4.4 kHz.(a) YIG/Pd.(b) YIG/Pt.(c) YIG/IrMn.

Kohler's rule for the MR [30, 31], namely, $MR = \Delta R/R \propto (M + \Delta M)^2 \approx M^2 + 2M\Delta M$, where ΔM is determined by the amplitude of the field modulation H_{mod}. The multiple-peaked structure results from the shape of the hysteresis cycle of the YIG magnetization and is characteristics of the magnetic response.

Figure 4 shows the experimental data for the magnetic field derivative of the resistance of the three YIG/ML samples measured with the field modulation technique. The same behavior measured with the magnetic field up and down shows that the resistance variation is symmetric relative to the applied magnetic field like the YIG hysteresis curve. It is interesting to note that the amplitude of the SMR signal decreases in the order Pd–Pt–IrMn, while the SPE-ISHE current peak amplitudes in figures 2(d)–(f) exhibit the opposite behavior. The multiple peak structure of the SMR data for all samples is clearly the same as in figure 3(b), demonstrating that the measured MRs follow Kohler's rule.

One difficulty for the calculation of the spin Hall angle from the SMR data is that according to equation (8) it depends crucially on the spin diffusion length of the ML, that for the materials investigated here has values in wide ranges as reported in the literature [3, 34]. Considering for Pt $\lambda_{ML} = 10.0$ nm and the average value for the SMR peak of $(0.62 \pm 0.002) \times 10^{-4}$, we obtain for the spin Hall angle $\theta_{SH\text{-}Pt} = (4.1 \pm 0.03)\%$. Similarly, using for λ_{ML} of Pd and IrMn, respectively, 3.0 nm and 5.0 nm, we obtain $\theta_{SH\text{-}Pd} = (3.1 \pm 0.03)\%$ and $\theta_{SH\text{-}IrMn} = (1.1 \pm 0.02)\%$. With the values of the spin Hall angles calculated from the SMR measurements, it is possible to write the following relation: $\theta_{SH\text{-}Pt} \approx 1.3 \times \theta_{SH\text{-}Pd} \approx 3.7 \times \theta_{SH\text{-}IrMn}$. Only for YIG/Pt sample is the spin Hall angle obtained from the SMR measurements similar to the one obtained with the SPE-ISHE technique. For the other ML materials there is a considerable

discrepancy between the values obtained from the two techniques. We attribute this discrepancy to the magnetic properties of Pd and IrMn that produces additional mechanisms for the MR [35–45]. In the case of Pd, according to the Stonerńs criterion [33], a thin ML film in close proximity with an FM material acquires ferromagnetic properties giving rise to an additional contribution for the MR [46]. In the case of IrMn, although ultrathin films do not have long range antiferromagnetic (AF) ordering, the short-range AF interaction associated with the interface exchange interaction affects its magneto-transport properties [43–45]. In summary, as IrMn does not have proximity effect, the spin Hall angle obtained by the ISHE ends up being greater than that obtained by SMR. On the other hand, as Pd has proximity effect the reverse effect occurs. This work also emphasizes our proposal for a new technique to measure the spin Hall angle. This technique has also been shown to be efficient in 2D materials [47].

5. Conclusions

We have investigated the spin-to-charge current conversion in YIG/ML (ML = Pd, Pt, IrMn) by two quite different techniques, SPE-ISHE, and modulated SMR. In both techniques the resulting effect is measured by the voltage produced along the ML through the ISHE. A simple model is presented to interpret the modulated SMR measurements that allows to obtain the spin Hall angles characterizing the spin-to-charge current conversion efficiency. The values of the spin Hall angle obtained with the two techniques, SPE-ISHE and SMR, are in good agreement for Pt, but not for Pd and IrMn. Possible reasons for the discrepancies in Pd and IrMn are discussed.

Acknowledgments

The authors are grateful to Professor Antonio Azevedo for providing the YIG film and for helpful discussions. This research was supported by Conselho Nacional de Desenvolvimento Científico e Tecnológico (CNPq); Coordenação de Aperfeiçoamento de Pessoal de Nível Superior (CAPES), Finance Code 001; Financiadora de Estudos e Projetos (FINEP); Fundação de Amparo à Ciência e Tecnologia do Estado de Pernambuco (FACEPE); Fundação de Amparo à Pesquisa do Estado de Minas Gerais (FAPEMIG) - Rede de Pesquisa em Materiais 2D and Rede de Nanomagnetismo.

Data availability statement

The data generated and/or analysed during the current study are not publicly available for legal/ethical reasons but are available from the corresponding author on reasonable request.

References

[1] Tserkovnyak Y, Brataas A and Bauer G E W 2002 Enhanced Gilbert damping in thin ferromagnetic films *Phys. Rev. Lett.* **88** 117601

[2] Hoffmann A 2013 Spin Hall effects in metals *IEEE Trans. Magn.* **49** 5172

[3] Sinova J, Valenzuela S O, Wunderlich J, Back C H and Jungwirth T 2015 Spin Hall effects *Rev. Mod. Phys.* **87** 1213

[4] Brataas A, van Wees B, Klein O, de Loubens G and Viret M 2020 Spin insulatronics *Phys. Rep.* **885** 1–27

[5] Hoffmann A and Bader S D 2015 Opportunities at the Frontiers of spintronics *Phys. Rev. Appl.* **4** 047001

[6] Hirsch J E 1999 Spin Hall effect *Phys. Rev. Lett.* **83** 1834

[7] Azevedo A, Vilela Leão L H, Rodríguez-Suárez R L, Oliveira A B and Rezende S M 2005 Dc effect in ferromagnetic resonance: evidence of the spin-pumping effect? *J. Appl. Phys.* **97** 10C715

[8] Mosendz O, Vlaminck V, Pearson J E, Fradin F Y, Bauer G E W, Bader S D and Hoffmann A 2010 Detection and quantification of inverse spin Hall effect from spin pumping in permalloy/normal metal bilayers *Phys. Rev.* B **82** 214403

[9] Sandweg C W, Kajiwara Y, Ando K, Saitoh E and Hillebrands B 2010 Enhancement of the spin pumping efficiency by spin wave mode selection *Appl. Phys. Lett.* **97** 252504

[10] Vilela-Leão L H, Salvador C, Azevedo A and Rezende S M 2011 Unidirectional anisotropy in the spin pumping voltage in yttrium iron garnet/platinum bilayers *Appl. Phys. Lett.* **99** 102505

[11] Hahn C, de Loubens G, Klein O, Viret M, Naletov V V and Ben Youssef J 2013 Comparative measurements of inverse spin Hall effects and magnetoresistance in YIG/Pt and YIG/Ta *Phys. Rev.* B **87** 174417

[12] Santos O A, Feringa F, Das K S, Youssef J B and van Wees B J 2021 Efficient modulation of magnon conductivity in $Y_3Fe_5O_{12}$ using anomalous spin Hall effect of a permalloy gate electrode *Phys. Rev. Appl.* **15** 014038

[13] Lustikova J, Shiomi Y and Saitoh E 2015 Vector spectroscopy for spin pumping *Phys. Rev.* B **92** 224436

[14] Zhang W, Jungfleisch M B, Jiang W, Pearson J E, Hoffmann A, Freimuth F and Mokrousov Y 2014 Spin Hall effects in metallic antiferromagnets *Phys. Rev. Lett.* **113** 196602

[15] Heinrich B, Burrowes C, Montoya E, Kardasz B, Girt E, Song Y-Y, Sun Y and Wu M 2011 Spin pumping at the magnetic insulator (YIG)/normal metal (Au) interfaces *Phys. Rev. Lett.* **107** 066604

[16] Mendes J B S, Alves Santos O, Meireles L M, Lacerda R G, Vilela-Leão L H, Machado F L A, Rodríguez-Suárez R L, Azevedo A and Rezende S M 2015 Spin-current to charge-current conversion and magnetoresistance in a hybrid structure of graphene and yttrium iron garnet *Phys. Rev. Lett.* **115** 226601

[17] Zhuravlev M Y, Vedyayev A V, Titova M S, Ryzhanova N V and Gusakova D 2017 Surface current at non-magnetic metal/ferromagnetic insulator interface due to Rashba spin–orbit interaction *J. Magn. Magn. Mater.* **441** 572–7

[18] Holanda J *et al* 2020 Magnetic damping modulation in $IrMn_3/Ni_{80}Fe_{20}$ via the magnetic spin Hall effect *Phys. Rev. Lett.* **124** 087204

[19] Kajiwara Y *et al* 2010 Transmission of electrical signals by spin-wave interconversion in a magnetic insulator *Nature* **464** 262

[20] Cornelissen L J, Liu J, Duine R A, Youssef J B and van Wees B J 2015 Long distance transport of magnon spin information in a magnetic insulator at room temperature *Nat. Phys.* **11** 1022

[21] Vidyasagar R *et al* 2016 Giant Zeeman shifts in the optical transitions of yttrium iron garnet thin films *Appl. Phys. Lett.* **109** 122402

[22] Huang S Y, Fan X, Qu D, Chen Y P, Wang W G, Wu J, Chen T Y, Xiao J Q and Chien C L 2012 Transport magnetic proximity effects in platinum *Phys. Rev. Lett.* **109** 107204

[23] Hoogeboom G R, Aqeel A, Kuschel T, Palstra T T M and van Wees B J 2017 Negative spin Hall magnetoresistance of Pt on the bulk easy-plane antiferromagnet NiO *Appl. Phys. Lett.* **111** 052409

[24] Wilhelm F *et al* 2000 Layer-resolved magnetic moments in Ni/Pt multilayers *Phys. Rev. Lett.* **85** 413
[25] Lin T, Tang C, Alyahayaei H M and Shi J 2014 Experimental investigation of the nature of the magnetoresistance effects in Pd-YIG hybrid structures *Phys. Rev. Lett.* **113** 037203
[26] Qiu Z, Ando K, Uchida K, Kajiwara Y, Takahashi R, Nakayama H, An T, Fujikawa Y and Saitoh E 2013 Spin mixing conductance at a well-controlled platinum/yttrium iron garnet interface *Appl. Phys. Lett.* **103** 092404
[27] Aqeel A, Vera-Marun I J, van Wees B J and Palstra T T M 2014 Surface sensitivity of the spin Seebeck effect *J. Appl. Phys.* **116** 153705
[28] Uchida K-i, Ohe J-i, Kikkawa T, Daimon S, Hou D, Qiu Z and Saitoh E 2015 Intrinsic surface magnetic anisotropy in $Y_3Fe_5O_{12}$ as the origin of low-magnetic-field behavior of the spin Seebeck effect *Phys. Rev.* B **92** 014415
[29] Mendes J B S, Cunha R O, Alves Santos O, Ribeiro P R T, Machado F L A, Rodríguez-Suárez R L, Azevedo A and Rezende S M 2014 Large inverse spin Hall effect in the antiferromagnetic metal $Ir_{20}Mn_{80}$ *Phys. Rev.* B **89** 140406(R)
[30] Mckenzie R H, Qualls J S, Han S Y and Brooks J S 1998 Violation of Kohler's rule by the magnetoresistance of a quasi-two-dimensional metal *Phys. Rev.* B **57** 11854
[31] Pippard A B 1989 *Magnetoresistance in Metals* (Cambridge: Cambridge University Press)
[32] Chen Y-T, Takahashi S, Nakayama H, Althammer M, Goennenwein S T B, Saitoh E and Bauer G E W 2013 Theory of spin Hall magnetoresistance *Phys. Rev.* B **87** 144411
[33] Rezende S M 2020 *Fundamentals of Magnonics* Lecture Notes in Physics vol 969 (Cham: Springer)
[34] Li M *et al* 2016 Spin orbit coupling controlled spin pumping and spin Hall magnetoresistance effects *Adv. Electron. Mater.* **2** 1600112
[35] Liang L, Chen Q, Lu J, Talsma W, Shan J, Blake G R, Palstra T T M and Ye J 2018 Inducing ferromagnetism and Kondo effect in platinum by paramagnetic ionic gating *Sci. Adv.* **4** eaar2030
[36] Acharyya R, Nguyen H Y T, Pratt W P and Bass J 2011 A study of spin–flipping in sputtered IrMn using Py-based exchange-biased spin-valves *J. Appl. Phys.* **109** 07C503
[37] Wang H, Du C, Hammel P C and Yang F 2017 Comparative determination of $Y_3Fe_5O_{15}$/Pt interfacial spin mixing conductance by spin-Hall magnetoresistance and spin pumping *Appl. Phys. Lett.* **110** 062402
[38] Holanda J, Maior D S, Alves Santos O, Vilela-Leão L H, Mendes J B S, Azevedo A, Rodríguez-Suárez R L and Rezende S M 2017 Spin Seebeck effect in the antiferromagnet nickel at room temperature *Appl. Phys. Lett.* **111** 172405
[39] Yang H X, Hallal A, Terrade D, Waintal X, Roche S and Chshiev M 2013 Proximity effects induced in graphene by magnetic insulators: first-principles calculations on spin filtering and exchange-splitting gaps *Phys. Rev. Lett.* **110** 046603
[40] Kim J, Sheng P, Takahashi S, Mitani S and Hayashi M 2016 Spin Hall magnetoresistance in metallic bilayers *Phys. Rev. Lett.* **116** 097201
[41] Nakayama H *et al* 2013 Spin Hall magnetoresistance induced by a nonequilibrium proximity effect *Phys. Rev. Lett.* **110** 206601
[42] Avci C O, Garello K, Ghosh A, Gabureac M, Alvarado S F and Gambardella P 2015 Unidirectional spin Hall magnetoresistance in ferromagnet/normal metal bilayers *Nat. Phys.* **11** 570
[43] Fischer J *et al* 2018 Spin Hall magnetoresistance in antiferromagnet/heavy-metal heterostructures *Phys. Rev.* B **97** 014417
[44] Zhou X, Ma L, Shi Z, Fan W J, Zheng J-G, Evans R F L and Zhou S M 2015 Magnetotransport in metal/insulating-ferromagnetheterostructures: spin Hall magnetoresistance or magnetic proximity effect *Phys. Rev.* B **92** 060402(R)
[45] Vélez S, Bedoya-Pinto A, Yan W, Hueso L E and Casanova F 2016 Competing effects at Pt/YIG interfaces: spin Hall magnetoresistance, magnon excitations, and magnetic frustration *Phys. Rev.* B **94** 174405
[46] Lu Y M, Choi Y, Ortega C M, Cheng X M, Cai J W, Huang S Y, Sun L and Chien C L 2013 Pt magnetic polarization on $Y_3Fe_5O_{12}$ and magnetotransport characteristics *Phys. Rev. Lett.* **110** 147207
[47] Mendes J B S, Rezende S M and Holanda J 2021 Rashba–Edelstein magnetoresistance in two-dimensional materials at room temperature *Phys. Rev.* B **104** 014408